Chapter 3

Structure and mechanical properties of UFG low carbon steel processed by ECAP followed by electropulsing

3.1 Introduction

Ultrafine-grained low carbon steel with significant mechanical properties is created through severe plastic deformation. However, these materials suffer from poor ductility [14,24] due to less dislocation activity and more non-equilibrium nature of boundaries, i.e., non-strain relaxed nature of grain boundaries [169]. The effects of electropulsing on the kinetics of recrystallization and plasticity enhancement have already been discussed in the literature section. There is a possibility of achieving a mixture of grain sizes by applying optimum pulsing conditions to obtain bimodal/ multimodal grain size distribution in SPD materials [47,170]. In this chapter, ECAPed low carbon steel is treated with EP for one pulse and repeatedly for five pulses in order to examine any changes in microstructural and mechanical properties.

3.2 Results

3.2.1 ECAP of D1 sample

The as-received hot-rolled low carbon steel contains 90% ferrite with an average grain size of 67 ± 12 μm and 10% fine pearlite (unresolved dark phase) as shown in the optical micrograph (Fig. 3.1a). The grain boundaries of the D1 sample are mostly high angle in nature (Fig. 3.1c) with an amount of 82%, and the remaining 18% consists of low angle grain boundaries. The D1 sample undergoes equal-channel angular pressing for ten passes (ε_{vM}=6), reducing the grain size to an ultrafine level, as shown in Figure 3.1c. During the ECAP process, additional LAGBs are created, accounting for 58% of the grain boundaries, as depicted in Figure 3.1d. After 10 passes of ECAP, both elongated and equiaxed grains are present, as shown in the TEM BF image in Figure 3.1e. The average grain size of at least 100 grains is measured to be 0.6±0.09 μm from the TEM BF images. Even though dynamic recovery has occurred in the ECAP-6 sample, there is still a high amount of dislocations persists inside the

material. Additionally, the SEM SEI image (Fig. 3.1f) of the ECAP-6 sample reveals the precipitation of fine carbides in the matrix phase.

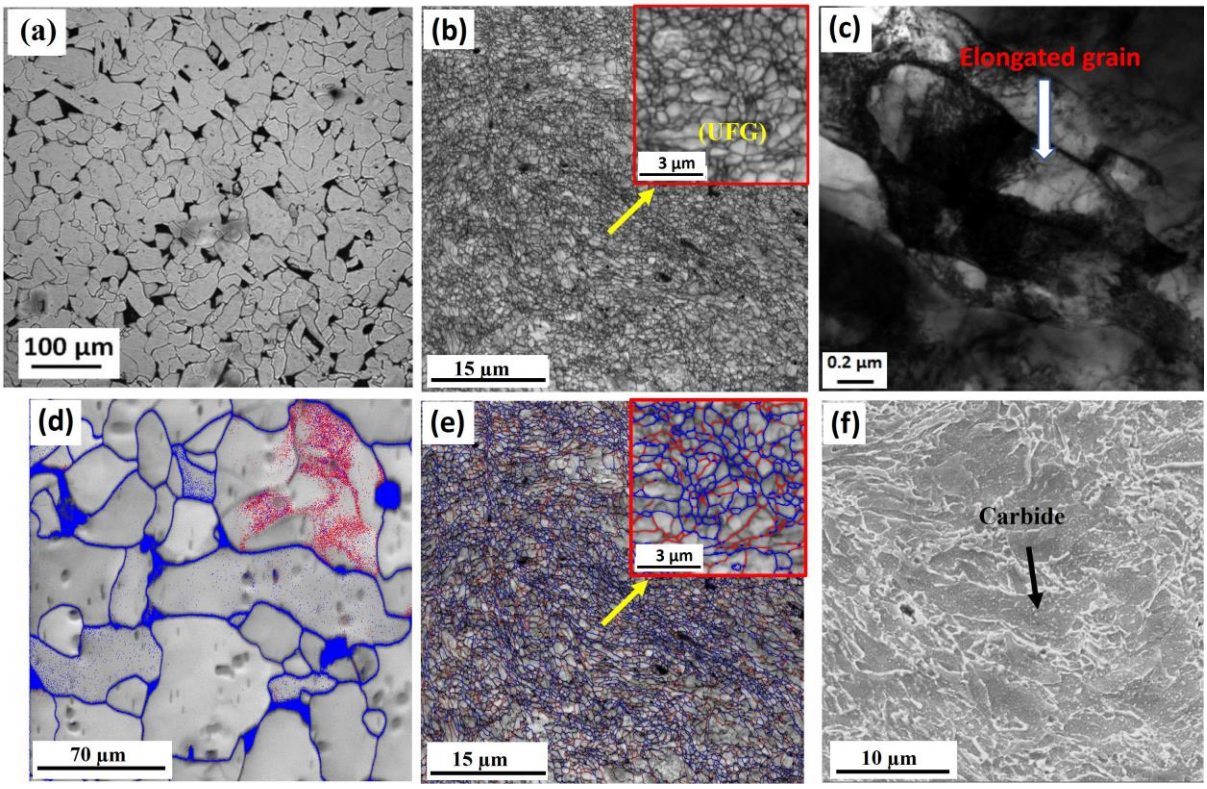

Figure 3.1. *(a) Optical micrograph of D1 sample, (b) IQ map of ECAP-6 sample, (c) TEM BF image of ECAP-6 sample, image quality maps with superimposed grain boundaries of (d) D1 and (e) ECAP-6 samples, blue lines for high angle grain boundaries (misorientation angle > 15°) and red lines for low angle boundaries (2° < misorientation angle < 15°) and (f) SEM SE micrograph of ECAP-6 sample. [In figures b and d, the insets are enlarged view of the indicated area]*

3.2.2 Electropulsing of ECAP-6 sample

The ECAP-6 sample is subjected to electropulsing and the processing parameters are already given in experimental section. The resulting damped sinusoidal wave form is shown in figure 3.2. Due to a large current density electropulsing generates heat that instantly raises temperature. The temperature rise (ΔT) due to Joule heating by EP can be expressed as given in the Equation 3.1 [171,172].

$$\Delta T = \frac{I^2 \Delta t \rho_r}{C_p d_m} \qquad (3.1)$$

where I is the current density, Δt is the pulse period of the first cycle, ρ_r is the electrical resistivity, C_p is the heat capacity of the material, and d_m is the density of the material. Substituting the values for I=14.25 × 10^9 A/m^2, Δt= 52 µs, ρ_r=1.65×10^{-7} Ωm, C_p=500 J/kg K and d_m=7.9×10^3 kg/m^3 in Equation 3.1 the calculated temperature rise is found to be 197 °C.

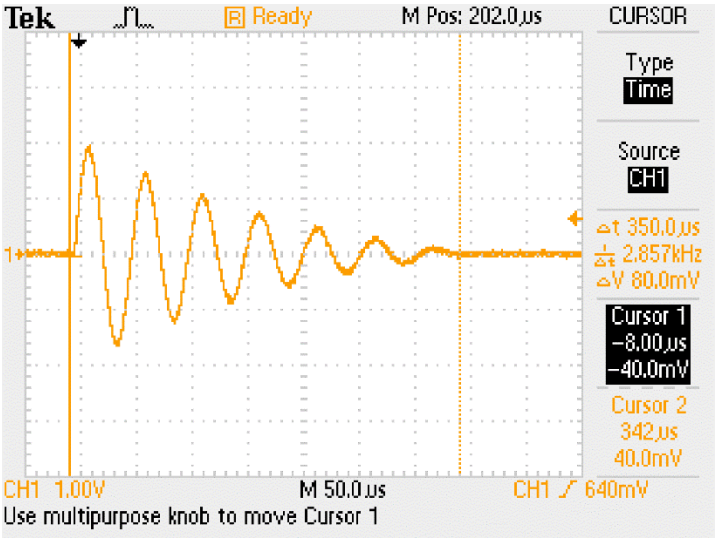

Figure 3.2. *Waveform of Electropulsing*

During electropulsing (ECAP-6-EP-1) of the ECAP-6 sample, bimodal grains with irregular sizes ranging from micron to ultrafine are produced, as shown in the SEM SEI image in Figure 3.3a. The bimodal distribution of grains is also evident in the EBSD IQ map, as depicted in Figure 3.3c and the magnified region. There is also a considerable decrease in the presence of fine carbides observed in the ECAP-6 sample after electropulsing, as shown in Figure 3.3a. After repeated pulsing (ECAP-6-EP-5), the SEM SEI image (Fig. 3.3b) shows that the grains have become equiaxed, and no carbides are observed between the grains. The equiaxed size of grains is further confirmed from the EBSD IQ map, as shown in Figure 3.3d.

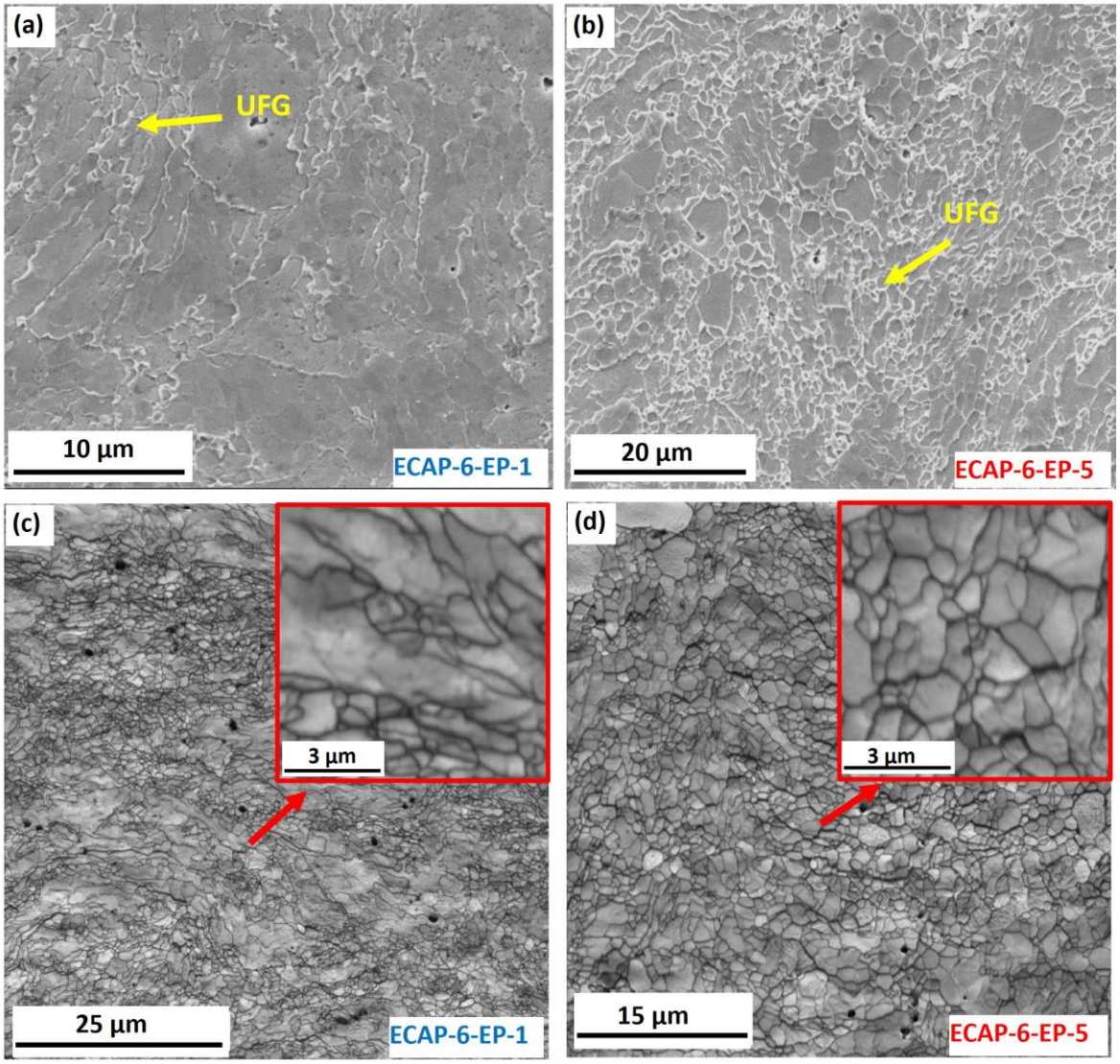

Figure 3.3. *SEM SEI of* ***(a)*** *ECAP-6-EP-1 and* ***(b)*** *ECAP-6-EP-5, IQ maps of* ***(c)*** *ECAP-6-EP-1 and* ***(d)*** *ECAP-6-EP-5.*

Figure 3.4a displays the IQ map of ECAP-6-EP-1, with superimposed blue lines representing HAGB (misorientation angles greater than 15°), and red lines indicating LAGB (misorientation angles between 2° and 15°). The IQ map reveals that the ECAP-6-EP-1 sample has a HAGB percent of 61% and a LAGB of 39%. The magnified region of the IQ map shows the migration of high angle boundaries influenced by the high-density current pulse and some other unstable HAGB created during ECAP are converted into LAGB. The TEM BF image (Fig. 3.4c) also shows sub-grain formation inside micron-sized grains. After undergoing repeated pulsing five times, the HAGB amount has marginally increased to 45%, as confirmed

by the EBSD IQ map (Fig. 3.4b). The TEM BF micrograph also shows the presence of equiaxed grains (indicated by the arrow in Fig. 3.4d) with relatively fewer dislocations, while the micron-sized grains (>10 µm in size) continue to be present.

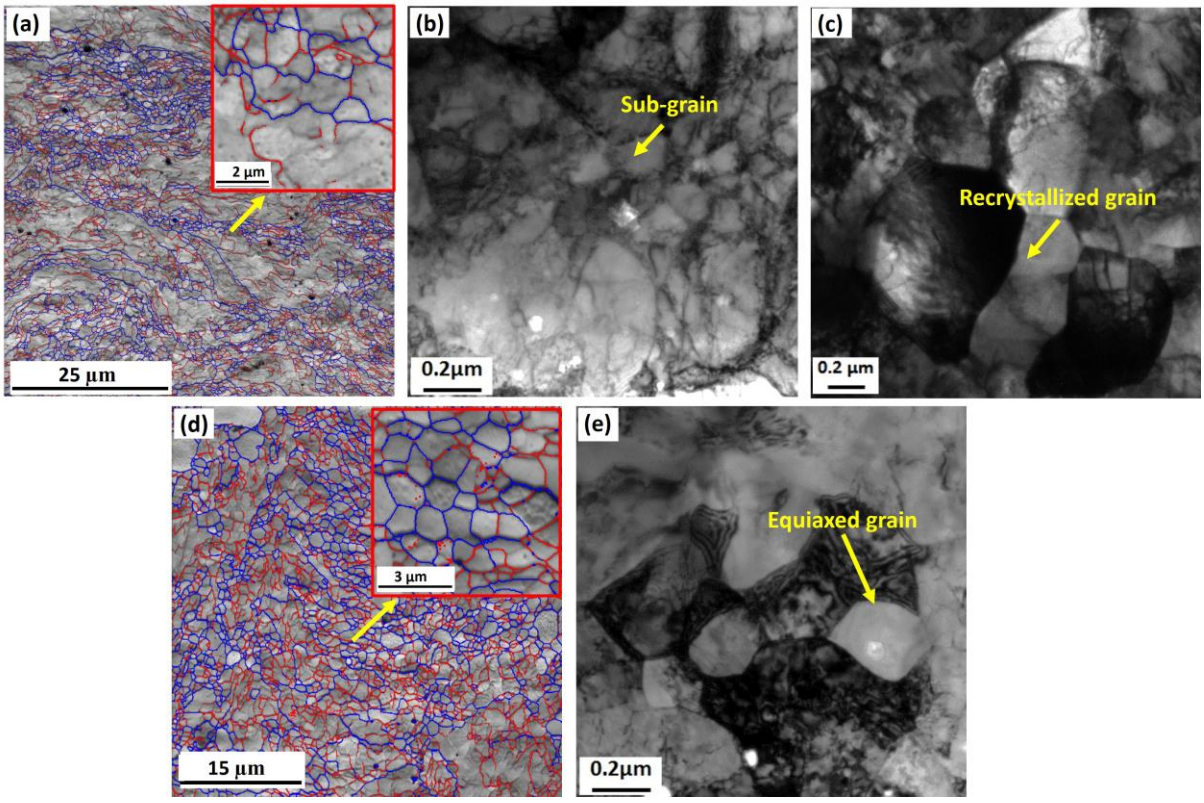

Figure 3.4. *EBSD IQ maps superimposed with grain boundaries (a) ECAP-6-EP-1 and (b) ECAP-6-EP-5 samples and TEM BF images of (c) ECAP-6-EP-1 and (d) ECAP-6-EP-5 (arrow shows an equiaxed grain) samples. (Blue and red lines delineate HAGB and LAGB respectively).*

The EBSD grain intercept distribution reveals that the average grain size of the D1 sample (Fig. 3.5a) is 52 µm when considering misorientation angles greater than 5° as grain boundaries. In contrast, the average grain size of the ECAP sample (ECAP-6) significantly decreases to 1.45 µm (Fig. 3.5b).

After one pulse (ECAP-6-EP-1), the grain size distribution shows that 50% of the grains have an average size of 15 µm, while the other 50% have an average size of 2 µm (Fig. 3.5c). Following five cycles of repetitive pulsing, the material exhibits a distribution with 50% of the

grains having an average size of 8.5 μm and the remaining 50% of grains having an average size of 1.8 μm (Fig. 3.5d).

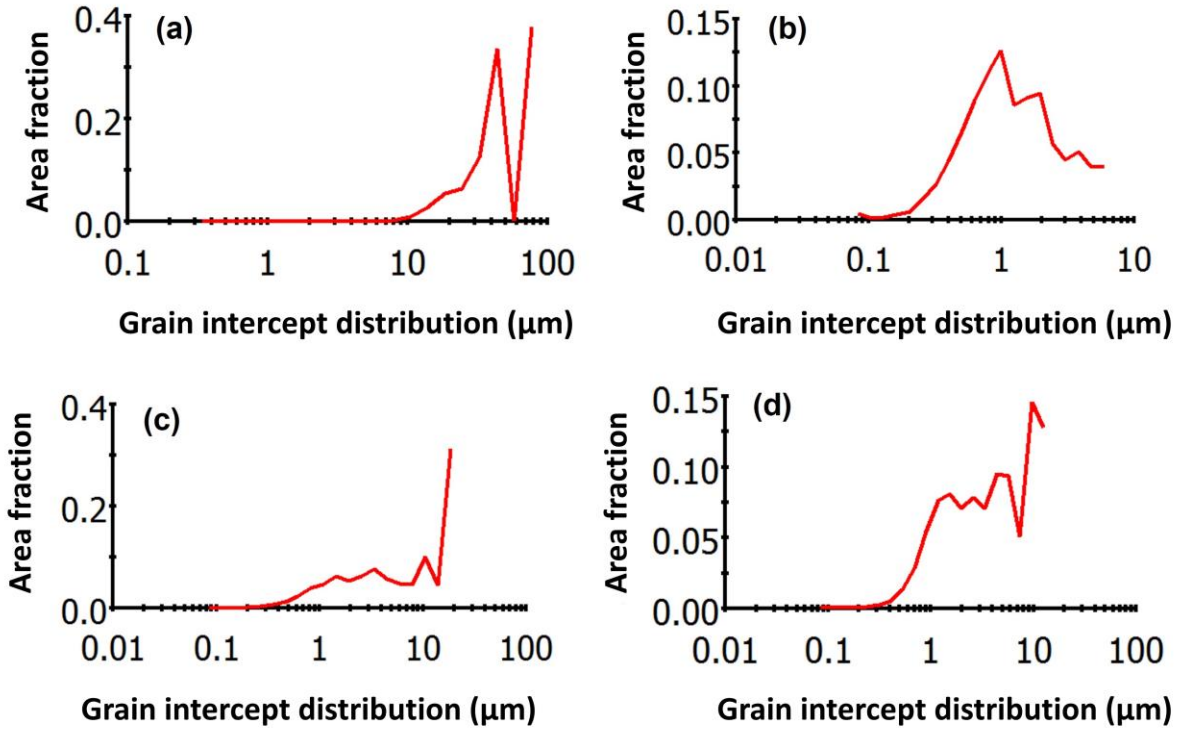

Figure 3.5. *EBSD grain intercept distributions (a) D1, (b) ECAP-6, (c) ECAP-6-EP-1 and (d) ECAP-6-EP-5.*

The grain boundaries are superimposed on the KAM map, considering misorientation angles between 0° and 5° as the lower and upper limits, respectively, as shown in Figure 3.6. The initial ECAP-6 sample (Fig. 3.6a) contains significant strain, along with a few recovered grains. However, after one pulse (ECAP-6-EP-1), a decrease in strain is observed in the material (Fig. 3.6b), indicating partial recrystallization. On repeated pulsing (ECAP-6-EP-5), the amount of strain is significantly reduced, as depicted in Figure 3.6c and its magnified region in Figure 3.6f. In this case, most of the grains are free of any strain, indicating the presence of recrystallized grains.

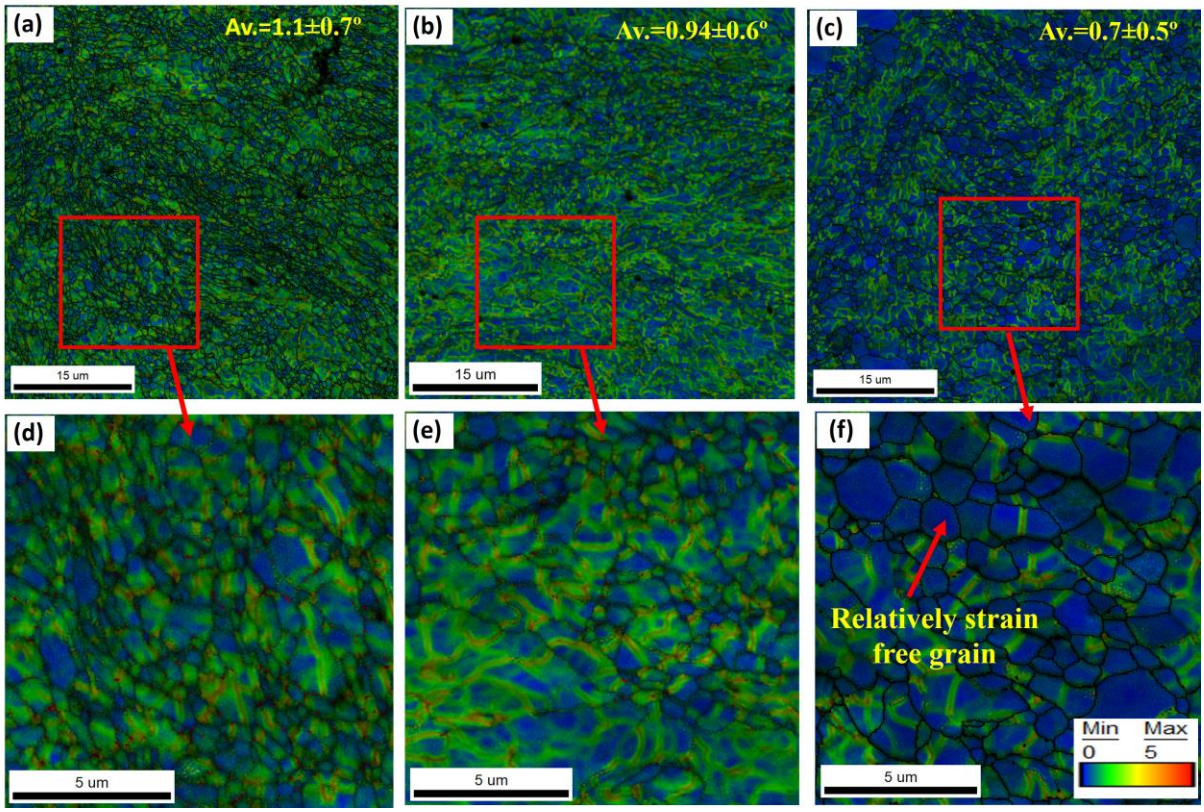

Figure 3.6. *Grain boundaries superimposed on EBSD KAM map in (a) ECAP-6 and its magnified region in (d), (b) ECAP-6-EP-1 and magnified region in (e) and (c) ECAP-6-EP-5 and magnified view in (f).*

Fig. 3.7a shows XRD peaks of the LCS-AR, ECAP-6, ECAP-6-EP-1 and ECAP-6-EP-5 samples. The presence of ferrite phase before and after EP is clearly observed. The magnified view of (110) is shown in Fig. 3.7b. It is observed that peak is broadened after ECAP of LCS-AR sample, however it is again decreased after pulsing. On the basis of the estimated temperature rise during EP, the ECAP-6 sample is annealed for 5 minutes (ECAP-6-H1) and 1 hour at 200 °C (ECAP-6-H2). The XRD peaks of these two materials are shown in Fig.3.7c.

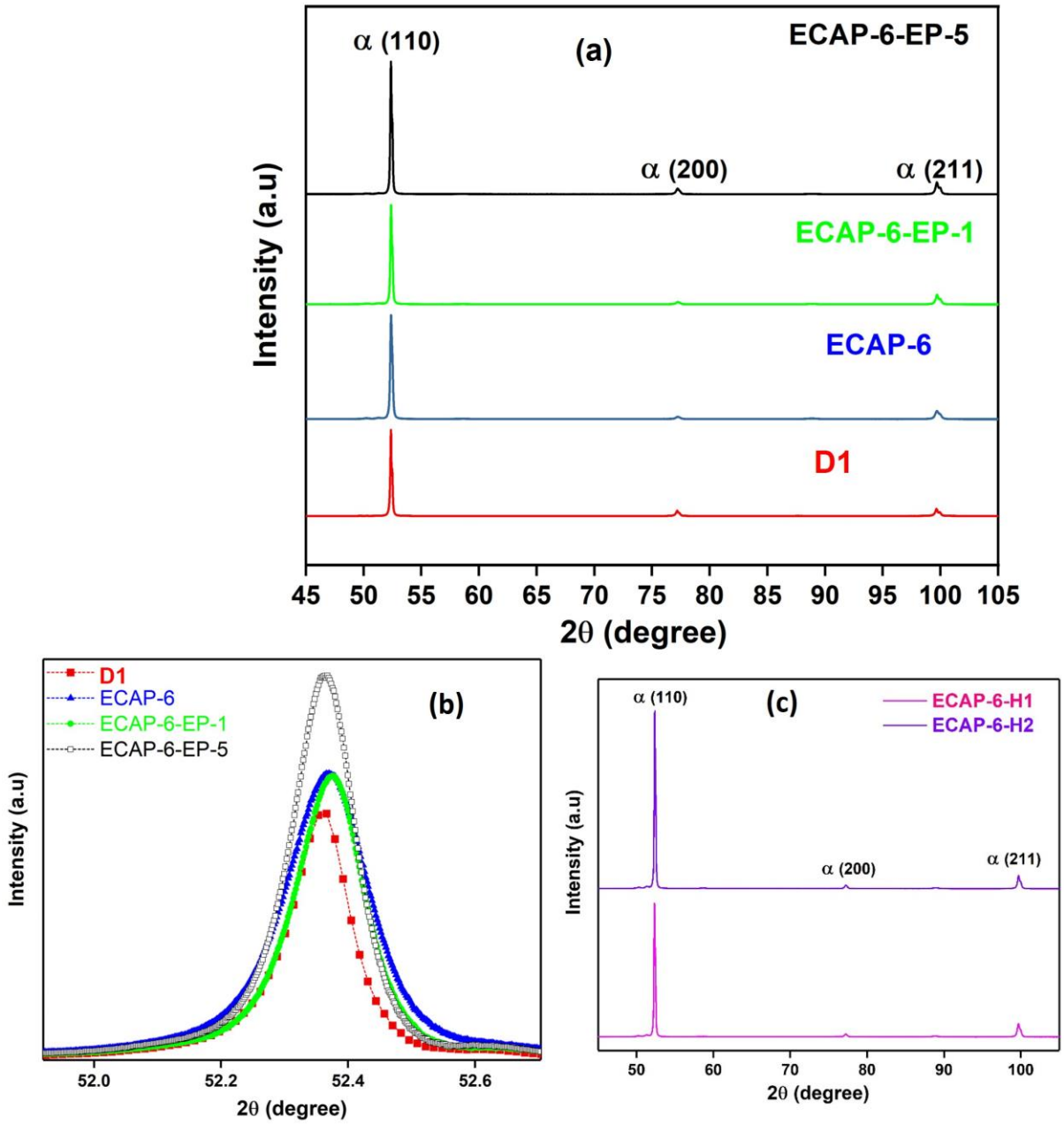

Figure 3.7. *(a) XRD peaks of LCS-AR, ECAP-6, ECAP-6-EP-1 and ECAP-6-EP-5, (b) magnified view of (111) and (c) XRD peaks of ECAP-6-H1, and ECAP-6-H2.*

The FWHM value of the samples is determined after fitting the peaks with Pseudo-Voigt function (Figure 3.8 a-f). The magnified view of (110) peak after fitting is shown within the micrographs. The red line shows experimental peaks and the blue line is after fitting with Pseudo-Voigt function. The differential plot between experimental and simulated curve is shown at the right side of every peak. The FWHM of D1 sample is found to be 0.11°, which

increases after ECAP (ECAP-6) to 0.16°. After EP, the FWHM again decreases with number of pulses (Table 3.1). However, annealing for five minutes (ECAP-6-H1) of ECAP sample does not show any significant change in FWHM value. Longer time annealing for one hour (ECAP-6-H2) shows FWHM value similar to ECAP-6-EP-1 sample, but it is lower than ECAP-6-EP-5. The crystallite size of ECAP-6 calculated to be 39 nm (Table 3.1). The crystallite size of ECAP-6-EP-1 and ECAP-6-EP-5 is increased to 48 nm and 52 nm respectively after electropulsing of ECAP-6 sample. ECAP-6 material shows a micro strain of 0.19 % which after on pulsing (ECAP-6-EP-1) decreases to 0.12 %. On electropulsing for five pulses (ECAP-6-EP-5), the micro strain decreases marginally to 0.11% (Table 3.1). The crystallite size of the 5 min annealed sample (ECAP-6-H1) is 45 nm, which is comparable to that of ECAP-6, however it increases in the 1 h annealed sample (ECAP-6-H2). The lattice strain, 0.15%, of short time annealed sample, ECAP-6-H1, is close to that of deformed sample, ECAP-6, but the lattice strain (0.13%) for the sample annealed for longer time decreases significantly.

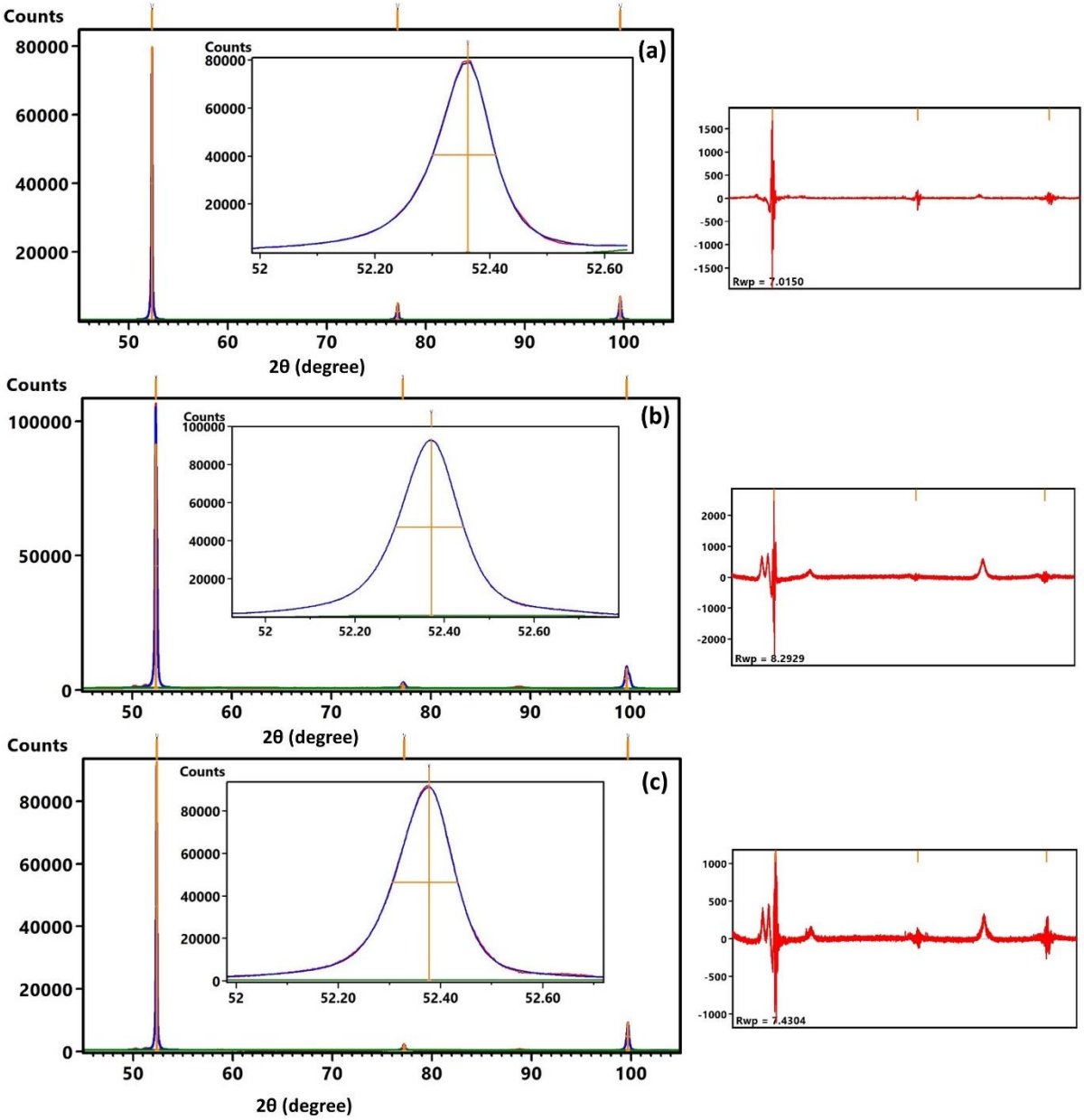

Figure 3.8. *(a) XRD peaks with magnified (110) of (a) D1, (b) ECAP-6, (c) ECAP-6-EP-1 (continue…)*

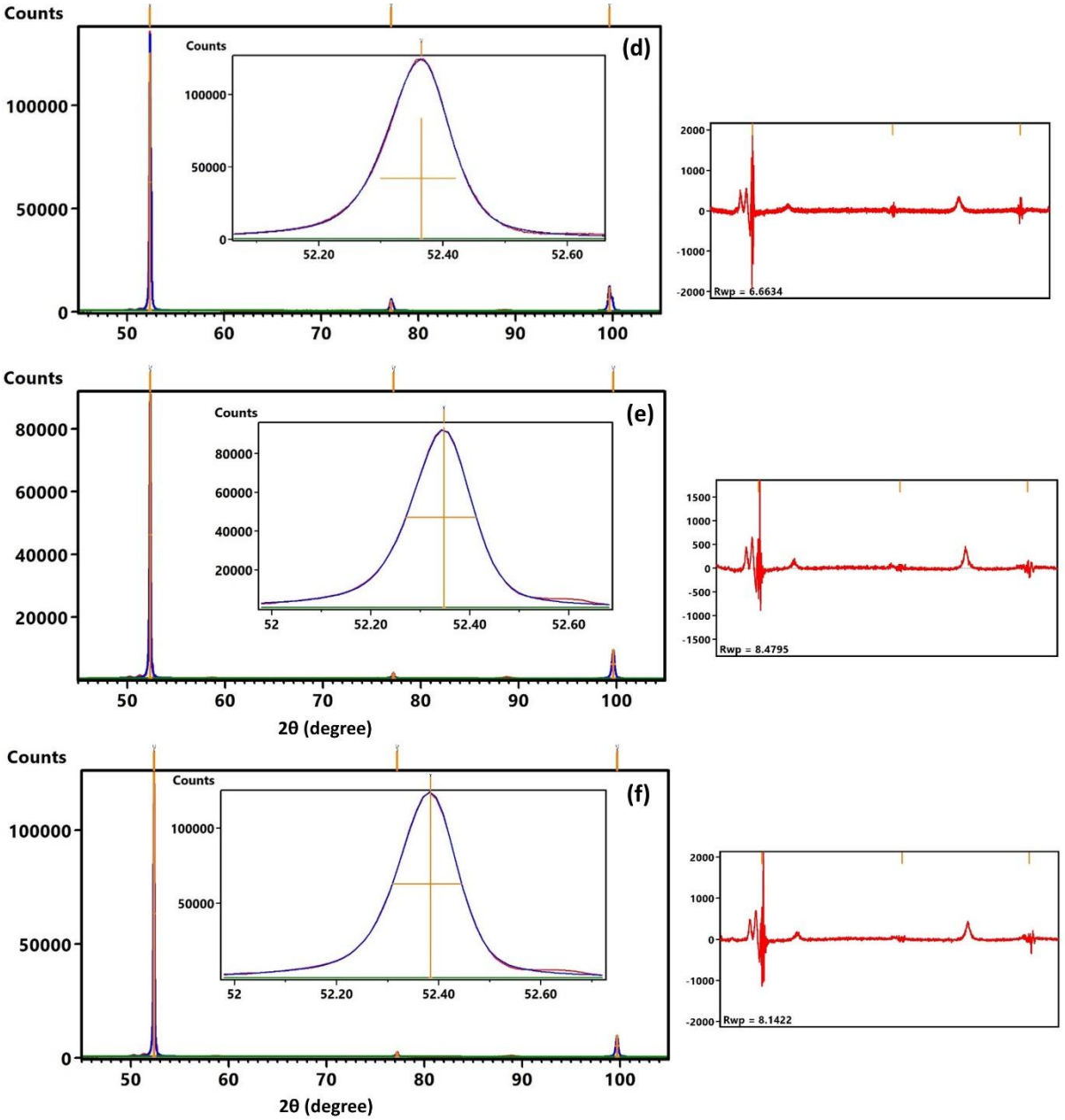

Figure 3.8. *(d) ECAP-6-EP-5 (e) ECAP-6-H1 and (f) ECAP-6-H2. Differential plot is shown at the right side of every XRD peak.*

The dislocation density of ECAP-6 sample calculated to be $5x10^{14}/m^2$. After electropulsing the dislocation density is decreased to $2x10^{14}/m^2$ and $1.5\ x10^{14}/m^2$ for ECAP-6-EP-1 and ECAP-6-EP-5 samples respectively. The dislocation density of short annealed sample (ECAP-6-H1) is calculated to be $4.5\ x10^{14}/m^2$, which is comparable to that of deformed sample. However, the dislocation density, $3.5\ x10^{14}/m^2$ of longer duration annealed sample (ECAP-6-

H2) is significantly lower than the deformed one. The details of crystallite size, lattice strain, and dislocation density are given in Table 3.1.

Table 3.1. Details of crystallite size, lattice strain, and dislocation density

Sample	FWHM of (110) (°)	Crystallite size (nm)	Strain (%)	Dislocation density x (10^{14}/m^2)
ECAP-6	0.16	39	0.19	5
ECAP-6-EP-1	0.13	48	0.12	2
ECAP-6-EP-5	0.12	52	0.11	1.5
ECAP-6-H1	0.16	45	0.15	4.5
ECAP-6-H2	0.13	51	0.13	3.5

The Vickers hardness of the D1 sample is measured to be 159 ± 4 HV [3]. After ECAP of low carbon steel, the hardness increases significantly to 220 ± 23 HV. However, after one pulse of electropulsing (ECAP-6-EP-1), the hardness slightly reduces to 200 ± 18 HV, and after five pulses, it decreases further to 162 ± 12 HV (Table 3.2). For the short-annealed sample (ECAP-6-H1), the hardness is 218 ± 7 HV, which is close to that of a deformed sample. However, for a longer duration annealed sample (ECAP-6-H2), the hardness significantly decreases to 208 ± 6 HV, lower than that of the deformed sample. The yield strength (YS) and ultimate tensile strength (UTS) of D1 sample are reported as 272 MPa and 367 MPa, respectively [14]. Following ECAP with an equivalent strain of 6 (ECAP-6), both the YS and UTS increase significantly to 625 MPa and 690 MPa, respectively (Fig. 3.9). However, after the ECAP-6 sample undergoes electropulsing for one pulse (ECAP-6-EP-1), the YS experiences a notable decrease, while the UTS is only marginally reduced. The D1 sample demonstrates uniform elongation (UE) and total elongation (TE) of 22% and 41%, respectively [14]. However, ECAP of LCS-AR at an equivalent strain of 6 (ECAP-6) results in reduced UE and TE, reaching 4% and 15%, respectively. By applying electropulsing to the ECAP-6 sample for one pulse (ECAP-6-EP-1), both UE and TE improve, reaching 7% and 20%, respectively. The details of tensile and hardness testing data are provided in Table 3.2.

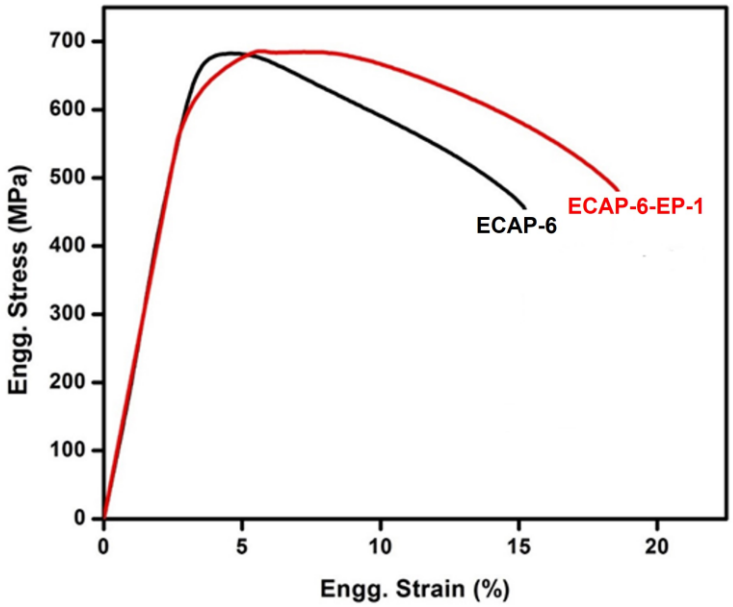

Figure 3.9. *Engineering stress vs. Engineering strain curves for ECAP-6 and ECAP-6-EP-1 samples.*

Table 3.2. Tensile and hardness testing results

Sample	Hardness (HV)	0.2% YS (MPa)	UTS (MPa)	Uniform Elongation (%)	Total Elongation (%)
D1 [14]	159±4	272	367	22	41
ECAP-6	220± 23	625	690	4	15
ECAP-6-EP-1	200± 18	522	686	7	20
ECAP-6-EP-5	162 ± 12				
ECAP-6-H1	218±7				
ECAP-6-H2	208±6				

3.3 Discussion

The application of severe plastic deformation through ECAP on low carbon steel, using a low imposed strain, leads to the division of grains into an elongated banded structure [14]. These bands exhibit a high dislocation density [173] , and their boundaries are characterized as diffusive or non-equilibrium in nature [174]. When an intermediate equivalent strain of 6 is

employed, the banded structure is preserved. Although the bands get subdivided due to the formation of sub-grains, the high dislocation density is still maintained, and the boundaries of the bands continue to exhibit a non-equilibrium nature.

Recent theories on EP accepts the combined thermal and athermal effects in the form of Joule heating and electron wind force respectively. These effects on the material are discussed in the current research separately.

3.3.1 Contribution of Joule heating towards grain modification

Due to the relatively low average temperature rise of only 197 °C and the high cooling rate imposed by the surrounding environment, it becomes impractical to achieve the phase transformation temperature or exceed the incubation period necessary for any phase change in the material. Moreover, this temperature is significantly below the recrystallization temperature of deformed ferritic steel.

The short-time annealed sample (ECAP-6-H1) subjected to a temperature of 200 °C for 5 minutes, falling within the range of electropulsing thermal effect, the dislocation density, crystallite size, and Vickers microhardness values closely resemble those of the deformed sample (ECAP-6). Hence, it is established that the short-duration thermal effect induced by electropulsing, which raises the average temperature to 197 °C, though local temperature rise is much higher but for a short duration, therefore, it does not significantly influence the material's properties. On the other hand, for a long-time heated sample (ECAP-6-H2) annealed at 200 °C for 1 hour, there is a significant reduction in dislocation density and hardness, along with an increase in crystallite size. This indicates that extended isothermal holding, which is not applicable for electropulsing conditions in the present experiment, can indeed modify the material's properties. So, the effect of EP which is for fractions second is nearly same as the

one-hour annealing at the same temperature. This indicates athermal effects of EP has a significant role for the microstructural modification.

3.3.2 Athermal effect of electropulsing

As thermal effects alone cannot account for the observed modifications in grain structure, athermal effects, such as the electric field and electron wind force [175], may play a significant role. When conducting electrons interact with impurities, vacancies, dislocations, and grain boundaries, they cause scattering in electrons. As a result of this scattering, energy is transferred to the material, leading to an increase in stress, strain, and diffusion rate [175,176].

During electropulsing, a large number of conducting electrons flow through the sample akin to a strong wind during a storm. This electron wind force refers to the force exerted on metal ions/atoms due to the momentum transfer from the conduction electrons. As a consequence of this force, atoms/ions move from metastable/unstable conditions towards a more stable configuration. The high current density of the electric pulse results in the drift electrons applying a force on the dislocations, referred to as the electron-wind force, which can be expressed by Equation (3.2) [175,177].

$$\tau_{ew} b = f_{ew}/l = IK_{ew} \qquad (3.2)$$

where τ_{ew} and f_{ew} are the stress and force acting on dislocation due to an electron wind, l is the length of dislocation and K_{ew} is the electron wind force coefficient. Putting the values of current density, Burgers vector (0.248 nm) and K_{ew}=2.65 × 10^{-12} N m/A [42], the load on dislocation per unit length due to electron wind force is found to be 152 MN/m.

The electric field generated during EP penetrates some specific grains (having an easy free-path for electrons). The high amount of dislocations generated during ECAP are pushed by the

electric wind force. The mobility of dislocations (M_d) is greatly enhanced and is given by Equation 3.3 [178].

$$M_d = M_a exp\left(\frac{-Q_{eff}}{kT}\right) \qquad (3.3)$$

where M_a is the pre-exponential factor dependent on the frequency of atom hopping and lattice distance, Q_{eff} is the effective kinetic barrier, k is the Boltzmann constant, and T is the temperature. When electric current is passed through the sample, the athermal effect changes the kinetic barrier for the dislocation movement. The effective barrier will be reduced as given in the Equation 3.3a [49].

$$Q_{eff} = Q - \Delta Q_{ath} \qquad (3.3a)$$

where Q is activation energy and ΔQ_{ath} is the activation energy change due to electric current. The activation energy change due to athermal effect is related to square root of current density as given in Equation 3.3b [49].

$$\Delta Q_{ath} = G\sqrt{I} \qquad (3.3b)$$

where I is current density and G is a constant. As current density increases, Q_{eff} decreases and indirectly mobility is increased.

The kinetic barrier for dislocation movement is greatly reduced in the presence of high-density current pulse [179]. The uneven distribution of electrons around the defects causes an anisotropic shielding effect to the electromagnetic forces between an atom and its neighbors. The additional diffusion flux due to electropulsing is given by Equation (3.4) [145,180].

$$J = \frac{2N_a e z^* D \rho_r I f \Delta t}{KT} \qquad (3.4)$$

where J is the additional atomic diffusion flux, N_a is the density of atoms, z^* is the effective valency of the Fe ion (=+3), D is lattice diffusion coefficient. As the frequency (f) and current

density (*I*) are very high in the present experiment (19.2 kHz and 14.25 kA/mm^2, respectively), the diffusion rate is expected to be enhanced significantly. Dislocations can move by three mechanisms, namely, climb, glide, and bowing. In the present case, due to thermal (Joule heating) and athermal (electron wind force) effects, there can be migration of dislocations in the material within a very short period.

The electropulsing process induces stresses for dislocation migration through athermal effects, such as compressive stress (due to rapid heating), pinch stress (due to magnetic force), and the electron wind effect (due to momentum transfer of conducting electrons to atoms' electrons, as well as the interaction of conducting electrons with phonons, referred to as the phonon effect). It is found in the present investigation that the average temperature rise of 473K (200°C) does not notably influence the changes in dislocation density. Similar experimental results by Suhong et al. [181] have shown the negligible effect of an average temperature rise of 373K (100°C) on the modification of persistent slip bands in a copper single crystal.

3.3.3 Effect of skin depth

When a high-frequency current is applied to a sample, the current distribution varies from the surface to the depth of the material. This phenomenon is known as the skin effect, and it becomes relevant in current electropulsing experiments due to the high frequency used (19.2 kHz). The skin depth (δ), which characterizes the penetration of the current into the material, can be calculated using Equation 3.5 [182].

$$\delta = \sqrt{\frac{\rho_r}{\pi f \mu_m}} \qquad (3.5)$$

where ρ_r is the resistivity, f is the frequency of EP, μ_m is the permeability (1.27 x 10^{-6} N/A^2). The skin depth is calculated to be about 2.6 mm. Since the calculated skin depth is higher than

the current sample thickness of 2 mm, it indicates that there is no possibility of localizing the current effect within the sample

3.3.4 Grain modification mechanism

After undergoing equal-channel angular pressing, the grains in the material become elongated into bands of sub-micron width, as seen in Figure 3.1c. Despite this transformation, the bands retain a high dislocation density and partial sub-grain structure within them, as depicted in Figure 3.1e.

During electropulsing for one pulse, the HAGB of the bands migrate due to the action of the electric field. Consequently, the bands tend to attain an equiaxed shape. The strong electron wind force enhances the mobility of dislocations, leading to the formation of sub-grain structures within the bands, and the existing sub-boundaries are pushed out. At this stage of electropulsing, a bimodal distribution of grain sizes is achieved, as shown in Figures 3.4a and 3.4c.

With further electropulsing, the migration of HAGB continues, resulting in the growth of larger grains. Some sub-grains coalesce with an increasing number of pulses, and the dislocations of LAGB sink into nearby HAGB, leading to the formation of defect-free regions. As the pulsing continues (up to 5 pulses), high angle boundaries of recrystallized grains impinge on each other and subsequently form a fine equiaxed microstructure, as observed in Figures 3.4b and 3.4d. Continuing the pulsing up to five pulses also result in a bimodal grain size distribution, but the resultant grain size is finer compared to that produced by a single pulse.

3.3.5 Mechanical properties

The strength and hardness of ECAPed low carbon steel are significantly higher than those of the coarse-grained as-received material (D1) due to grain refinement and the high dislocation density. However, the ductility of ultrafine-grained materials is lower because of

their limited work hardening ability, resulting from reduced dislocation activity in the grains [26].

Electropulsing the UFG material results in a selective increase in grain size to the micron level, leading to a bimodal distribution that includes a significant volume fraction of ultrafine grains. As a consequence, the strength and hardness of the material decrease marginally, while the yield strength is significantly reduced. Comparing this bimodal grain distribution with that produced by short-time annealing in copper [28], the electropulsed steel exhibits enhanced strength but less ductility. The strength of the electropulsed material is high compared to the short-time annealed material because the former contains more sub-grains, which effectively contribute to the Hall-Petch relationship. On the other hand, the annealed sample hardly contains any sub-grains inside a micron-sized grain [28,29]. In electropulsing, in addition to the migration of HAGB, dislocations are rearranged to create sub-grains. In contrast, secondary recrystallization only involves abnormal grain growth without the formation of sub-grains.

The hardness of a material is generally proportional to its yield strength, with a multiplying factor of approximately 3. This relationship explains the expected proportional decrease in both hardness and yield strength observed during electropulsing, as mentioned earlier. On the other hand, the ultimate tensile strength, which reflects the material's work hardening ability, remains relatively unchanged. Low YS and high UTS shows material has work hardened significantly. However, the ductility of the UFG ferritic steel is effectively recovered due to two main factors: a significant decrease in dislocation density and an increase in grain size to the micron level. As a result of the electropulsing process, a bimodal grain size distribution is achieved along with a reduction in defect density. These combined effects lead to a remarkable recovery in the material's ductility. Specifically, the uniform elongation increases by 3%, and the total elongation regains by 5%, even with just one pulse of electropulsing.

This demonstrates that electropulsing is effective in enhancing the ductility of ultrafine-grained ferritic steel, making it a valuable technique for improving the mechanical properties of such materials.

3.4 Conclusions

- Single-pulse electropulsing of low carbon steel processed by equal-channel angular pressing results in a bimodal distribution of grain sizes and a reduced defect density.
- When electropulsing is repeated, a few subgrains coalesce and grain boundaries migrate to impinge on each other, leading to the refinement of the microstructure and further reduction in defect density.
- Fine carbides that precipitate during ECAP is completely dissolved due to the accelerated movement of carbon atoms.
- Electropulsing of ultrafine-grained materials can enhance ductility by promoting the coarsening of some ultrafine grains into micron-sized grains through the migration of high-angle grain boundaries.
- Electropulsing of ECAPed low carbon steel results in a reduction in yield strength and hardness due to an increase in crystallite size, as well as a decrease in dislocation density and lattice strain.
- The work is of fundamental interest in revealing the consequences of applying electric pulses to deformed steel.